5786 *Chem. Mater.* **2010,** *22,* 5786–5796
DOI:10.1021/cm102147n

CHEMISTRY OF MATERIALS
Article

Novel n-Type Conjugated Ladder Heteroarenes: Synthesis, Self-Assembly of Nanowires, Electron Transport, and Electroluminescence of Bisindenoanthrazolines

Eilaf Ahmed,[†] Taeshik Earmme,[‡] Guoqiang Ren,[‡] and Samson A. Jenekhe*[,†,‡]

[†]*Department of Chemistry and* [‡]*Department of Chemical Engineering, University of Washington, Seattle, Washington 98195-1750*

Received July 31, 2010. Revised Manuscript Received September 1, 2010

A novel π-conjugated heptacyclic framework has been synthesized via a new one-step cyclization that results in a new class of n-type organic semiconductors. Single-crystal structures of bisindenoanthrazolines DADF and DADK showed that the π-conjugated heptacyclic framework is planar and leads to a slipped face-to-face π-stacking with short intramolecular distances (3.39 Å and 3.56 Å, respectively). The series of bisindenoanthrazolines have a formal reduction potential of −0.68 to −0.70 V (vs SCE) and an estimated electron affinity (LUMO level) of 3.65−3.72 eV. Electron mobility in evaporated thin films of the bisindenoanthrazolines, measured by the space-charge limited current method, was as high as 3.84×10^{-4} cm^2/(V s) under ambient air conditions. Organic light-emitting diodes based on DADA as the emissive material gave the best performance among the four molecules with a maximum brightness of 7610 cd/m^2, and maximum efficiency of 6.6 cd/A with EQE of 2.0% at a brightness of 936 cd/m^2. Phosphorescent organic light emitting diodes with *fac*-tris(2-phenylpyridine)iridium (Ir(ppy)$_3$) as the green triplet emitter and a bisindenoanthrazoline as the electron transport layer showed a brightness of 62 000 cd/m^2 and luminous efficiency of 39.2 cd/A at a brightness of 4270 cd/m^2. Nanowires of DADF and DADK self-assembled from solution were found to be single-crystalline and their morphology was further investigated by electron microscopy techniques. These results demonstrate the potential of bisindenoanthrazolines as new n-type semiconductors for organic electronics and optoelectronics.

1. Introduction

Organic semiconductors are of broad interest for applications in electronic and optoelectronic devices[1−20] such as photovoltaic cells,[1,2] light-emitting diodes,[3,20] and field-effect transistors.[4] Among the classes of organic semiconductors, large polycyclic heteroaromatics are of

*Corresponding author. E-mail: jenekhe@u.washington.edu.

(1) For recent reviews see: (a) Günes, S.; Neugebauer, H.; Sariciftci, N. S. *Chem. Rev.* **2007**, *107*, 1324. (b) Thompson, B. C.; Fréchet, J. M. J. *Angew. Chem., Int. Ed.* **2008**, *47*, 58. (c) Dennler, G.; Scharber, M. C.; Brabec, C. *J. Adv. Mater.* **2009**, *21*, 1323.

(2) (a) Halls, J. J. M.; Walsh, C. A.; Greenham, N. C.; Marseglia, E. A.; Friend, R. H.; Moratti, S. C.; Holmes, A. B. *Nature* **1995**, *376*, 498. (b) Alam, M. M.; Jenekhe, S. A. *Chem. Mater.* **2004**, *16*, 4647. (c) Liang, Y.; Xu, Z.; Xia, J.; Tsai, S.-T.; Wu, Y.; Li, G.; Ray, C.; Yu, L. *Adv. Mater.* **2010**, *22*, E135. (d) Wu, P.-T.; Bull, T.; Kim, F. S.; Luscombe, C. K.; Jenekhe, S. A. *Macromolecules* **2009**, *42*, 671. (e) Ren, G.; Wu, P.-T.; Jenekhe, S. A. *Chem. Mater.* **2010**, *22*, 2020.

(3) (a) Grimsdale, A. C.; Chan, K. L.; Martin, R. E.; Jokisz, P. G.; Holmes, A. B. *Chem. Rev.* **2009**, *109*, 897. (b) Shirota, Y.; Kageyama, H. *Chem. Rev.* **2007**, *107*, 953. (c) Jenekhe, S. A.; Lu, L.; Alam, M. M. *Macromolecules* **2001**, *34*, 7315. (d) Friend, R. H.; Gymer, R. W.; Holmes, A. B.; Burroughs, J. H.; Marks, R. N.; Taliani, C.; Bradly, D. D. C.; Dos Santos, D. A.; Brédas, J. L.; Lögdlund, M.; Salaneck, W. R. *Nature* **1999**, *397*, 121. (e) Kulkarni, A. P.; Gifford, A. P.; Tonzola, C. J.; Jenekhe, S. A. *Appl. Phys. Lett.* **2005**, *86*, 061106.

(4) (a) Coropceanu, V.; Cornil, J.; da Silva, D. A.; Olivier, Y.; Silbey, R.; Brédas, J.-L. *Chem. Rev.* **2007**, *107*, 926. (b) Murphy, A. R.; Fréchet, J. M. J. *Chem. Rev.* **2007**, *107*, 1066. (c) Zaumseil, J.; Sirringhaus, H. *Chem. Rev.* **2007**, *107*, 1296.

(5) (a) *Electronic Materials: The Oligomer Approach*; Müllen, K., Wegner, G., Eds.; Wiley-VCH: Weinheim, Germany, 1998. (b) Pope, M.; Swenberg, C. E. *Electronic Processes in Organic Crystals*; Oxford University Press: New York, 1999.

(6) (a) Scherf, U. *J. Mater. Chem.* **1999**, *9*, 1853. (b) Yang, C.; Scheiber, H.; List, E. J. W.; Jacob, J.; Müllen, K. *Macromolecules* **2006**, *39*, 5213. (c) Setayesh, S.; Marsitzky, D.; Müllen, K. *Macromolecules* **2000**, *39*, 2016.

(7) (a) Ahmed, E.; Briseno, A. L.; Xia, Y.; Jenekhe, S. A. *J. Am. Chem. Soc.* **2008**, *130*, 1118. (b) Mass-Torrent, M.; Hadley, P.; Bromley, S. T.; Ribas, X.; Tarrés, J.; Mas, M.; Molins, E.; Veciana, J.; Rovira, C. *J. Am. Chem. Soc.* **2004**, *126*, 8546.

(8) (a) Anthony, J. E. *Angew. Chem., Int. Ed.* **2008**, *47*, 452. (b) Anthony, J. E. *Chem. Rev.* **2006**, *106*, 5028. (c) Subramanian, S.; Park, S. K.; Parkin, S. R.; Podzorov, V.; Jackson, T. N.; Anthony, J. E. *J. Am. Chem. Soc.* **2008**, *130*, 2706. (d) Kim, D. H.; Lee, D. Y.; Lee, H. S.; Lee, W. H.; Kim, Y. H.; Han, J. I.; Cho, K. *Adv. Mater.* **2007**, *19*, 678. (e) Tang, M. L.; Reichardt, A. D.; Miyaki, N.; Stoltenberg, R. M.; Bao, Z. *J. Am. Chem. Soc.* **2008**, *130*, 6064.

(9) (a) Gao, P.; Beckmann, D.; Tsao, H. N.; Feng, X.; Enkelmann, V.; Baumgarten, M.; Pisula, W.; Müllen, K. *Adv. Mater.* **2009**, *21*, 213. (b) Gao, P.; Feng, X.; Yang; Enkelmann, V.; Baumgarten, M.; Müllen, K. *J. Org. Chem.* **2008**, *73*, 9207. (c) Takimiya, K.; Ebata, H.; Sakamoto, K.; Izawa, T.; Otsubo, T.; Kunugi, Y. *J. Am. Chem. Soc.* **2006**, *128*, 12604. (d) Ebata, H.; Izawa, T.; Miyazaki, E.; Takimiya, K.; Ikeda, M.; Kuwabara, H.; Yui, T. *J. Am. Chem. Soc.* **2007**, *129*, 15732. (e) Zhang, X.; Coté, A. P.; Matzger, A. J. *J. Am. Chem. Soc.* **2005**, *127*, 10502.

(10) (a) Boudreault, P.-L. T.; Wakim, S.; Blouin, N.; Simard, M.; Tessier, C.; Tao, Y.; Leclerc, M. *J. Am. Chem. Soc.* **2007**, *129*, 9125. (b) Boudreault, P.-L. T.; Wakim, S.; Tang, M. L.; Tao, Y.; Bao, Z.; Leclerc, M. *J. Mater. Chem.* **2009**, *19*, 2921. (c) Wakim, S.; Bouchard, J.; Blouin, N.; Michaud, A.; Leclerc, M. *Org. Lett.* **2004**, *6*, 3413. (d) Guo, Y.; Zhao, H.; Yu, G.; Di, C.-A.; Liu, W.; Jiang, S.; Yan, S.; Wang, C.; Zhang, H.; Sun, X.; Tao, X.; Liu, Y. *Adv. Mater.* **2008**, *20*, 4835.

Published on Web 09/29/2010

special interest because of their extended quasi-two-dimensional (2D) π-conjugation that results in planar backbone framework, improved intermolecular interactions, and improved thermal properties.[5−22] The vast majority of the literature to date has focused on the design, synthesis, and structure−property relationships of *p*-type organic semiconductors,[5−10] including: oligoacenes,[8] fused oligothiophenes,[9] anthradithiophenes,[8] bisindolocarbazoles,[10] oligophenylenes, and oligofluorenes,[6,11] some of which have resulted in field-effect transistors with performance superior to amorphous silicon.[8] In contrast, the development of *n*-type oligomer and polymer semiconductors has lagged behind *p*-type materials.[12−24] A common strategy in the design of n-type organic semiconductors is the substitution of hydrocarbons with electron-deficient moieties such as fluorine,[12,13,25] cyano groups,[14−17] carbonyls,[15] and/or imine nitrogens.[19−24] Among n-type ladder oligomers studied to date are perfluorinated oligoacenes[25] and thiophenes,[26] oligoindenofluorenes,[11,15] naphthalene diimides,[13,17,18] perylene diimides,[16,27] and imine nitrogen-rich oligomers.[19−24] The design and synthesis of new n-type organic semiconductors is necessary for understanding structure−property relationships in the materials and for improving their performance in organic electronics and optoelectronics.

Ladder polycyclic aromatic molecules that contain imine nitrogens are of increasing interest in the development of *n*-type semiconductors.[14−24] Incorporation of imine nitrogens into ladder-type conjugated oligomers can result in: (i) an increase in electron affinity;[19−24] (ii) enhancement of the propensity of π-stacking;[21−24] (iii) ability to tune the electronic and optoelectronic properties by protonation or metal ion complexation;[21a,b,22a] and (iv) a substantial improvement in photo-oxidative stability of the molecules. Experimental[14−23] and theoretical[24] studies have shown that heteroaromatic rings containing imine nitrogens have higher reduction potential compared to similar hydrocarbons. Theoretical studies have also showed that linear expansion of size in such imine nitrogen-containing polycyclic molecules is very beneficial toward increasing the reduction potential[24] and reducing intrinsic energy barriers and trapping centers that cause low carrier mobility.[28a,b] Examples of such an extension of the size of π-conjugated polycyclic molecules and incorporation of imine nitrogens and/or heteroatoms to increase the reduction potentials include core-expanded perylene bisimides,[29] quinoxaline and pyrazinoquionoxaline derivatives,[21,22] bisphenazine derivatives,[23] and indenofluorenes/bisindenofluorenes derivatives.[11,15]

Also of fundamental and technological interest is the synthesis of one-dimensional (1D) nanostructures of organic semiconductors.[30−33] Self-assembly of organic semiconductors into well-defined 1D nanostructures such as nanowires or nanobelts represent a successful approach

(11) (a) Jacob, J.; Sax, S.; Piok, T.; List, E. J. W.; Grimsdale, A. C.; Müllen, K. *J. Am. Chem. Soc.* **2004**, *126*, 6987. (b) Zhou, Y.; Liu, W.-J.; Ma, Y.; Wang, H.; Qi, L.; Cao, Y.; Wang, J.; Pei, J. *J. Am. Chem. Soc.* **2007**, *129*, 12386.
(12) Bao, Z.; Lovinger, A. J.; Brown, J. *J. Am. Chem. Soc.* **1998**, *120*, 207.
(13) (a) Katz, H. E.; Lovinger, A. J.; Johnson, J.; Kloc, C.; Seigrist, T.; Li, W.; Lin, Y.-Y.; Dodablapur, A. *Nature* **2000**, *404*, 478. (b) Katz, H. E.; Johnson, J.; Lovinger, A. J.; Li, W. *J. Am. Chem. Soc.* **2000**, *122*, 7787.
(14) (a) Handa, S.; Miyazaki, E.; Takimiya, K.; Kunugi, Y. *J. Am. Chem. Soc.* **2007**, *129*, 11684. (b) Pappenfus, T. M.; Chesterfield, R. J.; Frisbie, C. D.; Mann, K. R.; Casado, J.; Raff, J. D.; Miller, L. L. *J. Am. Chem. Soc.* **2002**, *124*, 4184.
(15) (a) Usta, H.; Facchetti, A.; Marks, T. J. *Org. Lett.* **2008**, *10*, 1385. (b) Usta, H.; Risko, C.; Wang, Z.; Huang, H.; Deliomeroglu, M. K.; Zhukhovitskiy, A.; Facchetti, A.; Marks, T. J. *J. Am. Chem. Soc.* **2009**, *131*, 5586.
(16) Jones, B. A.; Ahrens, M. J.; Yoon, M. H.; Facchetti, A.; Marks, T. J.; Wasielewski, M. R. *Angew. Chem., Int. Ed.* **2004**, *43*, 6363.
(17) Jones, B. A.; Facchetti, A.; Wasielewski, M. R.; Marks, T. J. *Chem. Mater.* **2007**, *19*, 2703.
(18) (a) Kim, F. S.; Guo, X.; Watson, M. D.; Jenekhe, S. A. *Adv. Mater.* **2010**, *22*, 478. (b) Yan, H.; Chen, Z.; Zhen, Y.; Newman, C.; Quinn, J. R.; Dötz, F.; Kastler, M.; Facchetti, A. *Nature* **2009**, *457*, 679.
(19) (a) Babel, A.; Jenekhe, S. A. *J. Am. Chem. Soc.* **2003**, *125*, 13656. (b) Babel, A.; Jenekhe, S. A. *Adv. Mater.* **2002**, *14*, 371.
(20) (a) Tonzola, C. J.; Alam, M. M.; Kaminsky, W.; Jenekhe, S. A. *J. Am. Chem. Soc.* **2003**, *125*, 13548. (b) Kulkarni, A. P.; Tonzola, C. J.; Babel, A.; Jenekhe, S. A. *Chem. Mater.* **2004**, *16*, 4556. (c) Tonzola, C. J.; Kulkarni, A. P.; Gifford, A. P.; Kaminsky, W.; Jenekhe, S. A. *Adv. Funct. Mater.* **2007**, *17*, 863. (d) Kulkarni, A. P.; Jenekhe, S. A. *Macromolecules* **2003**, *36*, 5285. (e) Zhang, X.; Shetty, A. S.; Jenekhe, S. A. *Macromolecules* **1999**, *32*, 7422.
(21) (a) Jenekhe, S. A. *Macromolecules* **1991**, *24*, 1. (b) Miao, S.; Bromobosz, S. M.; Schleyer, P. v. R.; Wu, J. I.; Barlow, S.; Marder, S. R.; Hardcastle, K. I.; Bunz, U. H. F. *J. Am. Chem. Soc.* **2008**, *130*, 7339. (c) Nishida, J.-I.; Naraso; Murai, S.; Fujiwara, E.; Tada, H.; Tomura, M.; Yamashita, Y. *Org. Lett.* **2004**, *6*, 2007. (d) Kaafarani, B. R.; Kondo, T.; Yu, J.; Zhang, Q.; Dattilo, D.; Risko, C.; Jones, S. C.; Barlow, S.; Domercq, B.; Amy, F.; Kahn, A.; Brédas, J.-L.; Kippelen, B.; Marder, S. R. *J. Am. Chem. Soc.* **2005**, *127*, 16358.
(22) (a) Fogel, Y.; Kastler, M.; Wang, Z.; Andrienko, D.; Bodwell, G. J.; Müllen, K. *J. Am. Chem. Soc.* **2007**, *129*, 11743. (b) Lee, D.-C.; Jang, K.; McGrath, K. K.; Uy, R.; Robins, K. A.; Hatchett, D. W. *Chem. Mater.* **2008**, *20*, 3688. (c) Gao, B.; Wang, M.; Jing, X.; Wang, F. *J. Am. Chem. Soc.* **2008**, *130*, 8297. (d) Zhu, Y.; Yen, C.-T.; Jenekhe, S. A.; Chen, W.-C. *Macromol. Rapid Commun.* **2004**, 25–1829.
(23) Nakagawa, T.; Kumaki, D.; Nishida, J.-I.; Tokito, S.; Yamashita, Y. *Chem. Mater.* **2008**, *20*, 2615.
(24) Winkler, M.; Houk, K. N. *J. Am. Chem. Soc.* **2007**, 129–1805.
(25) (a) Sakamoto, Y.; Suzuki, T.; Kobayashi, M.; Gao, Y.; Fukai, Y.; Inoue, Y.; Sato, F.; Tokito, S. *J. Am. Chem. Soc.* **2004**, *126*, 8138. (b) Tang, M. L.; Reichardt, A. D.; Wei, P.; Bao, Z. *J. Am. Chem. Soc.* **2009**, *131*, 5264.
(26) (a) Facchetti, A.; Yoon, M.-H.; Stern, C. L.; Hutchison, G. R.; Ratner, M. A.; Marks, T. J. *J. Am. Chem. Soc.* **2004**, *126*, 13480. (b) Wang, Y.; Parkin, S. R.; Gierschner, J.; Watson, M. D. *Org. Lett.* **2008**, *10*, 3307.
(27) (a) Chesterfield, R. J.; McKeen, J. C.; Newman, C. R.; Ewbank, P. C.; daSilva; Filho, D. A.; Brédas, J.-L.; Miller, L. L.; Mann, K. R.; Frisbie, C. D. *J. Phys. Chem. B* **2004**, *108*, 19281. (b) Schemidt, R.; Oh, J. H.; Sun, Y.-S.; Deppisch, M.; Krause, A.-M.; Radacki, K.; Braunschweig, H.; Könemann, M.; Erk, P.; Bao, Z.; Würthner, F. *J. Am. Chem. Soc.* **2009**, *131*, 6215.
(28) (a) Norton, J. E.; Brédas, J.-L. *J. Am. Chem. Soc.* **2008**, *130*, 12377. (b) Verlaak, S.; Heremans, P. *Phys. Rev. B: Condens. Matter. Mater. Phys.* **2007**, *75*, 115127/1. (c) Ruiz Delgade, M. C.; Kim, E.-G.; da Silva Filho, D. A.; Brédas, J.-L. *J. Am. Chem. Soc.* **2010**, *132*, 3375.
(29) (a) Tsao, H. N.; Wojciech, P.; Liu, Z.; Osikowicz, W.; Salaneck, W. R.; Müllen, K. *Adv. Mater.* **2008**, *20*, 2715. (b) Avlasevich, Y.; Müller, S.; Erk, P.; Müllen, K. *Chem.—Eur. J.* **2007**, *13*, 6555. (c) Qian, H.; Negri, F.; Wang, C.; Wang, Z. *J. Am. Chem. Soc.* **2008**, *130*, 17970.
(30) For recent reviews see: (a) Schenning, A. P. H. J.; Meijer, E. W. *Chem. Commun.* **2005**, 3245. (b) Würthner, F. *Chem. Commun.* **2004**, *14*, 1564. (c) Zang, L.; Che, Y.; Moore, J. S. *Acc. Chem. Res.* **2008**, *41*, 1596. (d) Briseno, A. L.; Mannsfeld, S. C. B.; Jenekhe, S. A.; Bao, Z.; Xia, Y. *Mater. Today* **2008**, *11*, 38.
(31) (a) Xin, H.; Kim, F. S.; Jenekhe, S. A. *J. Am. Chem. Soc.* **2008**, *130*, 5424. (b) Xin, H.; Ren, G.; Kim, F. S.; Jenekhe, S. A. *Chem. Mater.* **2008**, *20*, 6199. (c) Xin, H.; Reid, O. G.; Ren, G.; Kim, F. S.; Ginger, D. S.; Jenekhe, S. A. *ACS Nano* **2010**, *4*, 1861.

Chart 1. Molecular Structures of Bisindenoanthrazolines

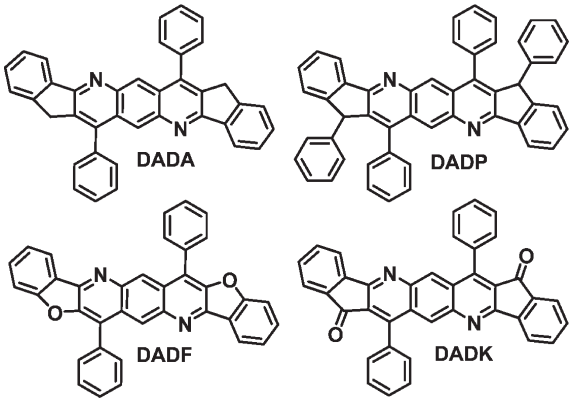

to controlling the solid-state morphology for structure−property studies and elucidation of charge transport mechanisms at the nanoscale and for electronic and optoelectronic devices.[30−33] Despite the significant advances in molecular design[1−23]and their widespread applications in organic electronics and optoelectronics,[1−20] only a few n-type organic or polymer semiconductors have been successfully explored as 1D nanostructures.[22b,32]

In this paper, we report the synthesis, crystal structures, electrochemical properties, photophysics, self-assembly of nanowires, electron-transport, and light-emitting properties of novel ladder-type bisindenoanthrazolines (BIDAs). The molecular structures of the four bisindenoanthrazolines (DADA, DADP, DADF, and DADK) investigated are shown in Chart 1. The series of BIDAs has a common framework of a highly planar heptacyclic ring that contains a core of anthrazoline ring with two imine nitrogens in the backbone. Various substitutions were examined toward tuning the electronic properties and solid-state structures. The simplicity and flexibility of the synthesis allows for the retention of n-type characteristics while tuning the electronic structures and intermolecular interactions by simple substitutents (X = methylene, benzyl, carbonyl, and ether). We discovered that small changes in the molecular structures result in drastic effects on both the solid-state packing and the electronic and optoelectronic properties.

Structure−property relationships of the bisindenoanthrazolines were investigated by X-ray single crystals, cyclic voltammetry, photophysical measurements, space-charge limited current (SCLC) measurements of electron mobility, and electroluminescent devices. Single-crystal X-ray diffraction showed that BIDAs are fused heptacyclics with a highly planar and rigid framework. The new n-type materials had reversible electrochemical reductions from which an electron affinity of 3.6−3.7 eV was estimated. We also report the solution-phase self-assembly of nanowires of some of the molecules (DADF and DADK).

2. Experimental Section

2.1. Materials. All commercially available reagents were purchased from Sigma-Aldrich and used without further purification.

Synthetic Procedures. 2,5-Dibenzoyl-1,4-diphenylenediamine was synthesized according to the known literature method.[7a]

General Procedure for Synthesis of BIDAs. A mixture of 2,5-dibenzoyl-1,4-diphenylenediamine (1.0 equiv.), indanone-functionalized compound (2.1 equiv.) and diphenyl phosphate (8 equiv.) in 5 mL of toluene were refluxed in inert atmosphere for 12 h. The reaction mixture was precipitated from 10% methanol/triethylamine and the solid was collected by vacuum filteration. The resulting product was recrystallized from THF/MeOH.

DADA. A mixture of indanone (0.53 g, 4.0 mmol), 2,5-dibenzoyl-1,4-diphenylenediamine (0.6 g, 1.89 mmol), and diphenyl phosphate were refluxed in toluene. DADA was extracted and purified according to the above general procedure in 96% yield as a yellow solid. ^{1}H NMR (300 MHz, $CDCl_3$): δ ppm = 8.677 (s, 2H), 8.303 (d, 2H), 7.674−7.606 (m, 10H), 7.530 (m, 6H), 3.943 (s, 4H). ^{13}C NMR (TFA-d_6): δ ppm 160.00, 153.70, 150.38, 137.50, 134.07, 131.67, 131.27, 130.59, 129.53, 128.59, 128.21, 126.39, 124.55, 34.04. HRMS (FAB) calcd for $C_{38}H_{24}N_2$, 508.19395; found M+, 508.19418.

DADP. A mixture of 3-phenyl-1-indanone (0.69 g, 3.3 mmol), 2,5-dibenzoyl-1,4-diphenylenediamine (0.5 g, 1.58 mmol), and diphenyl phosphate were refluxed in toluene overnight. DADP was extracted and purified according to the above general procedure to give a yellow solid in 91% yield. ^{1}H NMR (300 MHz, $CDCl_3$): δ ppm = 8.5271 (s, 2H), 8.2989 (d, 2H), 7.575−7.402 (m, 12H), 7.159 (t, 2 H), 6.694 (d, 2H), 6.579 (d, 2H), 5.217 (s, 2H). ^{13}C NMR (TFA-d_6): δ ppm = 160.41, 155.51, 154.57, 142.19, 138.14, 135.19, 134.06, 131.16, 130.45, 129.96, 129.70, 129.56, 129.28, 128.65, 128.49, 128.04, 127.81, 127.57, 126.77, 124.15, 119.46. HRMS (FAB) calcd for $C_{50}H_{32}N_3$, 660.25387; found M+, 660.25469.

DADF. A mixture of 2H-benzofuran-3-one (0.466 g, 3.48 mmol), 2,5-dibenzoyl-1,4-diphenylenediamine (0.5 g, 1.58 mmol), and diphenyl phosphate were refluxed in toluene overnight. DADF was extracted and purified according to the above general procedure to give an orange solid in 85% yield. ^{1}H NMR (300 MHz, TFA-d_6): δ ppm = 9.519 (s, 2H), 8.586 (d, 2H), 8.220 (t, 2H), 8.022−7.907 (m, 12H), 7.803 (t, 2H). ^{13}C NMR (TFA-d_6): δ ppm = 163.39, 139.79, 139.39, 132.53, 132.16, 130.08, 129.44, 127.61, 126.42, 124.62, 120.09, 115.83, 114.53, 113.54. HRMS (FAB) calcd for $C_{36}H_{20}N_2O_2$, 513.1603; found M+, 513.16092.

DADK. A mixture of 1,3-indanedione (0.509 g, 3.48 mmol), 2,5-dibenzoyl-1,4-diphenylenediamine (0.5 g, 1.58 mmol), and diphenyl phosphate were refluxed in toluene. DADA was extracted and purified according to the above general procedure in 90% yield as an orange solid. ^{1}H NMR (300 MHz, TFA-d_6): δ ppm = 8.999 (s, 2H), 8.454−8.427 (m, 2H), 8.184−8.079 (m, 6H), 7.957−7.841 (m, 6H), 7.704−7.677 (m, 4H). ^{13}C NMR (TFA-d_6): δ ppm = 186.07, 157.50, 138.81, 138.53, 137.90, 135.89, 133.49, 132.37, 131.94, 129.14, 128.79, 128.17, 126.18, 125.81, 125.55, 124.45. HRMS (FAB) calcd for $C_{38}H_{20}N_2O_2$, 537.1603; found M+, 537.16054.

(32) (a) Briseno, A. L.; Mannsfeld, S. C. B.; Reese, C.; Hancock, J. M.; Xiong, Y.; Jenekhe, S. A.; Bao, Z.; Xia, Y. *Nano Lett*. **2007**, *7*, 2847. (b) Che, Y.; Datar, A.; Balakrishnan, K.; Zang, L. *J. Am. Chem. Soc*. **2007**, *129*, 7234. (c) Balakrishnan, K.; Datar, A.; Oitker, R.; Chen, H.; Zuo, J.; Zang, L. *J. Am. Chem. Soc*. **2005**, *127*, 10496. (d) Lee, D.-C.; McGrath, K. K.; Jang, K. *Chem. Commun*. **2008**, 3636. (e) Briseno, A. L.; Mannsfeld, S. C. B.; Shamberger, P. J.; Ohuchi, F.; Bao, Z.; Jenekhe, S. A.; Xia, Y. *Chem. Mater*. **2008**, *20*, 4712.

(33) (a) Briseno, A. L.; Mannsfeld, S. C. B.; Ling, M.; Liu, S.; Tseng, R. J.; Reese, C.; Roberts, M.; Yang, Y.; Wudl, F.; Bao, Z. *Nature* **2006**, *444*, 913. (b) de Boer, R. W. I.; Gershenson, M. E.; Morpurgo, A. F.; Podzorov, V. *Phys. Stat. Solidi(a)* **2004**, *201*, 1302. (c) Gershenson, M. E.; Podzorov, V.; Morpurgo, A. F. *Rev. Mod. Phys*. **2006**, *78*, 973.

2.2. Characterization. ^{1}H NMR spectra were recorded on a Bruker AV300 at 300 MHz using deuterochloroform ($CDCl_3$) or deuterotrifluoroacetic acid (CF_3COOD) as the solvent. Mass spectra were obtained from JEOL/HX-110 using 2-nitrophenyloctylether as a matrix. Thermogravimetric analysis of the molecules was conducted on a TA Instruments model Q50 TGA. A heating rate of 10 °C/min under a flow of N_2 was used with runs conducted from room temperature to 500 °C. Cyclic voltammetry was done on an EG&G Princeton Applied Research potentiostat/galvanostat (model 273A). Data were analyzed by using a Model 270 Electrochemical Analysis System Software on a PC computer. A three-electrode cell was used, using platinum wire electrodes as both counter and working electrode. Silver/silver ion (Ag in 0.1 M $AgNO_3$ solution, Bioanalytical System, Inc.) was used as a reference electrode. Ferrocene/ferrocenium (Fc/Fc^+) was used as an internal standard. The potential values obtained in reference to Ag/Ag^+ were converted to the saturated calomel electrode (SCE) scale. Solution cyclic voltammetry was performed in 1 mM solution of the compound in a mixed 1,2-dichlorobenzene/acetonitrile (10:3 v/v) solvent containing 0.1 M $TBAPF_6$ as electrolyte at 100 °C. All solutions were purged with N_2 for 20 min before each experiment. UV−vis absorption spectra were collected on a Perkin-Elmer model Lambda 900 UV/vis/near-IR spectrophotometer. The photoluminescence (PL) emission spectra were obtained with a Photon Technology International (PTI) Inc. model QM2001−4 spectrofluorimeter.

2.3. Fabrication and Characterization of OLEDs. We fabricated multilayer OLEDs using the bisindenoanthrazolines as an emitter. ITO-coated glass substrates (10 Ω/sq, Shanghai B. Tree Tech. Consult Co., Ltd., Shanghai, China) were cleaned sequentially in ultrasonic baths of acetone, deionized water, and isopropanol, and then dried at 60 °C in a vacuum oven overnight. The commercially available 1 wt % dispersion of PEDOT:PSS (Clevios PVP Al 4083 H.C. Starck) in water was used after it was filtered through 0.45 μm GHP syringe filters. A 50 nm thick PEDOT:PSS layer was spin-coated on top of ITO glass and dried at 150 °C under a vacuum to get rid of residual water molecules. A 10−20 nm thick TAPC (1,1-bis-(di-4-tolylaminophenyl)-cyclohexane) hole-transport/electron-blocking layer was spin-coated from its 0.3−0.5 wt % toluene solution onto the PEDOT:PSS layer and dried at 60 °C overnight under vacuum. A 20 nm thick film of each bisindenoanthrazoline was obtained on top of TAPC layer by evaporation from resistively heated quartz crucibles at a rate of ca. 0.1−0.3 nm/s in a vacuum evaporator (Edwards Auto 306) at base pressure of $< 7 \times 10^{-7}$ Torr. When TPBI (1,3,5-tris(N-phenylbenzimidizol-2-yl)benzene) was used, it was evaporated right after evaporation of bisindenoanthrazoline. Then LiF and Al were sequentially deposited onto the organic layer without breaking vacuum.

To investigate phosphorescent organic light-emitting diodes (PhOLEDs) using bisindenoanthrazolines as an ETL, we fabricated green phosphorescent organic light-emitting diodes (PhOLEDs) using blends of poly(*N*-vinylcarbazole) (PVK) and 1,3-bis(2-(4-*tert*-butylphenyl)-1,3,4-oxadiazo-5-yl)benzene (OXD-7) (PVK:OXD-7 = 60:40 wt/wt) as the host doped with 1.0 wt % *fac*-tris-(2-phenylpyridine)iridium ($Ir(ppy)_3$) as the green triplet emitter in the EML. For the hole injection layer, a solution PEDOT:PSS was spin-coated to make a 30 nm thick layer onto a precleaned ITO glass and annealed at 150 °C under vacuum. A 70 nm thick EML was obtained by spin-coating of the PVK:OXD-7:$Ir(ppy)_3$ blend in chlorobenzene onto the PEDOT:PSS layer and vacuum-dried at 100 °C. A 20 nm bisindenoanthorazolines followed by LiF and Al cathode are then thermally vacuum evaporated to obtain the device structures: ITO/PEDOT:PSS/EML/BIDA/LiF/Al.

Film thickness was measured by an Alpha-Step 500 profilometer (KLA-Tencor, San Jose, CA). EL (Electroluminescence) spectra were obtained using the same spectrofluorimeter in photophysical properties. Current−voltage characteristics of the OLEDs were measured by using a HP4155A semiconductor parameter analyzer (Yokogawa Hewlett-Packard, Tokyo). The luminance was simultaneously measured by using a model 370 optometer (UDT Instruments, Baltimore, MD) equipped with a calibrated luminance sensor head (Model 211) and a 5× objective lens. The device external quantum efficiencies were calculated by using procedures reported previously.[20d,e] All the device fabrication and device characterization steps were carried out under ambient laboratory condition.

Devices for space-charge limited current (SCLC) measurement were fabricated with Al/bisindenoanthrazolines/Al structure. The Al electrode and organic layer were obtained by the same evaporation method as the fabrication of OLED devices. Current−voltage characteristics of SCLC devices were measured using the same semiconductor parameter analyzer as for OLED devices. The measurements were performed under dark and ambient conditions.

3. Results and Discussion

3.1. Synthesis and Characterization. The bisindenoanthrazoline framework contains seven-fused rings, including 5 hexagons and 2 pentagons. The synthesis of the heptacyclic bisindenoanthrazolines involved a cyclization reaction of 2,5-dibenzoyl-1,4-phenylenediamine (**1**) as outlined in Scheme 1. The four BIDAs were synthesized in high yield via Friedlander condensation using diphenyl phosphate (DPP) as an acid catalyst. The DPP catalyst was readily removed by precipitation into a 10% triethylamine/methanol solution.[34] DADA, DADP, DADF, and DADK were recrystallized from 1:1 THF:MeOH solvent mixture. ^{1}H NMR spectra, ^{13}C NMR spectra, and high resolution mass spectrometry of the molecules and X-ray single-crystal determination on two of them confirmed the structures. The four BIDAs are soluble in common organic solvents (chloroform, toluene, dichlorobenzene, etc.) to varying degrees. Thin-films of the molecules were easily obtained by vacuum deposition. The decomposition temperatures are in the range of 418−498 °C as determined by thermogravimetric analysis (TGA). Glass transition temperature and melting points were not observed by differential scanning calorimetry (DSC) up to 300 °C.

3.2. Crystal Structures and Morphology. Single crystals of DADF and DADK were grown by physical vapor transport sublimation.[33] Single-crystal X-ray diffraction was performed to investigate the solid-state packing and the intermolecular interactions in the new organic semiconductors. DADF forms a monoclinic primitive lattice with a space group of $P21/n$ and unit-cell dimensions of a = 14.3821(5) Å, b = 4.73830(10) Å, c = 18.2103(8) Å, $\alpha = 90°$, $\beta = 99.5260°$ (12), and $\gamma = 90°$. Single-crystal X-ray diffraction of DADK also showed a monoclinic primitive lattice with a space group of $P21/C$ and the

(34) (a) Agrawal, A. K.; Jenekhe, S. A. *Macromolecules* **1991**, *24*, 6806. (b) Agrawal, A. K.; Jenekhe, S. A. *Macromolecules* **1993**, *26*, 895.

Scheme 1. Synthesis of Bisindenoanthrazolines

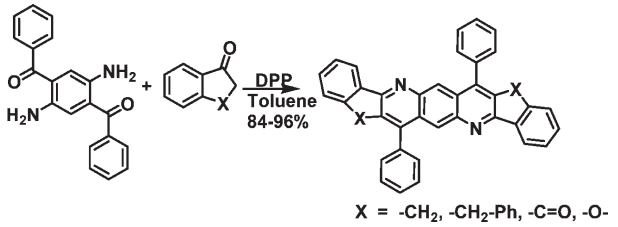

Table 1. Crystallographic Data for DADF and DADK

	DADF	DADK
formula	$C_{36}H_{20}N_2O_2$	$C_{38}H_{20}N_2O_2$
fw	512.54	536.56
cryst syst	monoclinic	monoclinic
color of cryst	orange	yellow
space group	*P*21/n	*P*21/*c*
a (Å)	14.3821 (5)	7.1904(3)
b (Å)	4.73830(10)	27.9435 (5)
c (Å)	18.2103(8)	13.7000(15)
α (deg)	90	90
β (deg)	99.5260(12)	108.4290(14)
γ (deg)	90	90
V (Å^3)	1223.75(7)	2611.4(3)
T (K)	418 (2)	292 (2)
Z	2	4
R_f	0.0558	0.0618
R_w	0.1449	0.1667
GOF	1.079	0.999

unit-cell dimensions are $a = 7.1904(3)$ Å, $b = 27.9435(5)$ Å, $c = 13.7000(15)$ Å, $\alpha = 90°$, $\beta = 108.429°$ (12), and $\gamma = 90°$ (Table 1). The crystal structure of both molecules reveals that the seven fused rings are relatively planar and that the phenyl rings of DADF have a twist angle of 60° compared to 68° in the case of DADK, as shown in the thermal ellipsoid plot in Figures 1A and 2A, respectively.

The molecular packing diagram in Figure 1B shows that DADF forms a slipped face-to-face π-stacking along the *b*-axis and edge-to-face interactions in the 101 direction. The shortest intermolecular distance between adjacent molecules is 3.56 Å. The inset in Figure 1B shows the distance of the phenyl groups in the 001 direction and the imine nitrogens of the molecules that lie in the 010 plane (C−N) is 3.6 Å. Figure 1C is similar to Figure 1B, with molecules along the 001 deleted to clearly show the π-stacking along the *b*-axis. Contrary to the π-stacking motif in DADF, DADK forms a slipped face-to-face π-stacking along the *a*-axis, as shown in the molecular packing diagram in Figure 2C. The shortest intermolecular distance between adjacent molecules is 3.39 Å. Figure 2B shows multiple short intermolecular distances between adjacent molecules in DADK; the phenyl rings were deleted for clarity. It is clear that the substitution with carbonyl group results in much shorter and thus stronger intermolecular interactions.

Although we were unable to grow suitable single crystals of DADA and DADP for X-ray single-crystal diffraction, it can be expected from the single-crystal structures of DADF and DADK that DADA and DADP have similarly a planar backbone. However, it is likely that these BIDAs have larger intermolecular distances

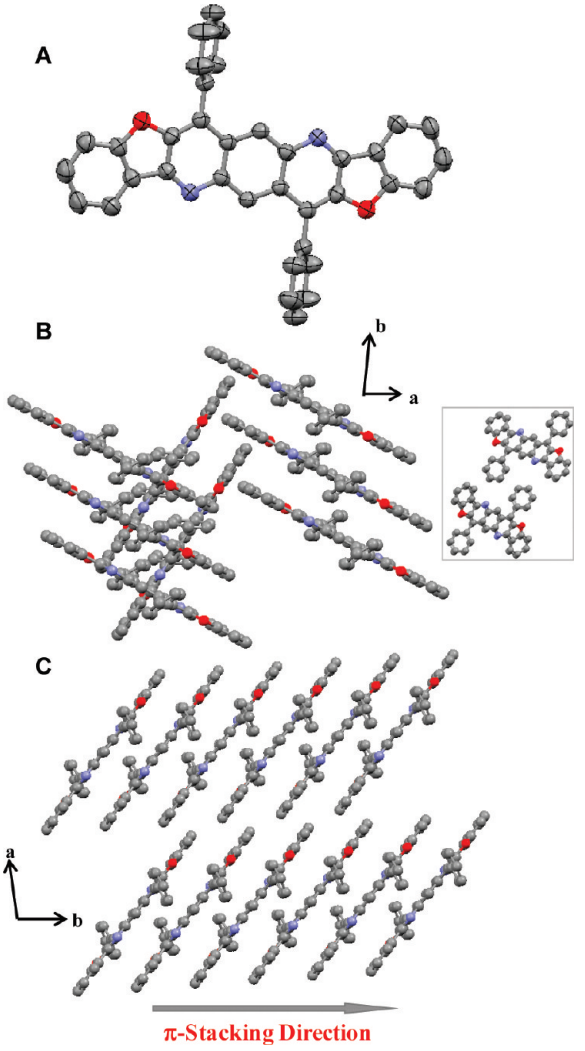

Figure 1. Single-crystal X-ray structure of DADF (A) Thermal ellipsoid plot with ellipsoids drawn at 50% probability level. (B) Face-to-face π-stacking of two DADF molecules with shortest intermolecular distance of 3.63 Å. (C) Molecular packing of DADF illustrating π-stacking direction, view down the *c*-axis.

than those in DADK and DADF. The highly planar backbone of the BIDAs clearly results in shorter intermolecular distances and thus better π-orbital overlap between adjacent molecules compared to previously reported tricyclic anthrazolines.[20a]

3.3. Photophysics. Figure 3A shows the normalized absorption spectra of the four bisindenoanthrazolines in dilute tetrahydrofuran (THF) solutions. The spectra show two bands, a lower-intensity band in the range of 340−410 nm and a higher-intensity band in the 280−310 nm range. These absorption bands in DADA, DADP, and DADF spectra are associated with $\pi-\pi^*$ transitions. However, the lowest-energy absorption band in DADK is due to $n-\pi^*$ transition, whereas the higher energy band is from $\pi-\pi^*$ transition. All the solution absorption spectra show clear vibronic structures, indicative of well-defined rigid chromophores. All the BIDA molecules except DADF show an absorption maximum that corresponds to the 0−1 optical transition (the highest oscillator strength). The absorption maximum of DADF

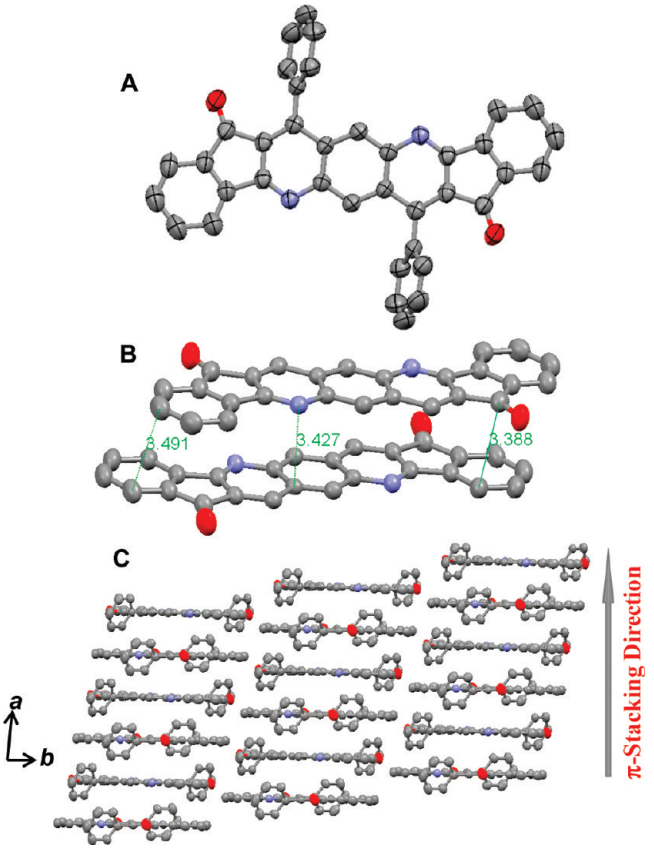

Figure 2. Single-crystal X-ray structure of DADK (A) Thermal ellipsoid plot with ellipsoids drawn at 50% probability level. (B) Face-to-face π-stacking of two DADK molecules with shortest intermolecular distance of 3.39 Å. (C) Molecular packing of DADK illustrating π-stacking direction, view down the *c*-axis.

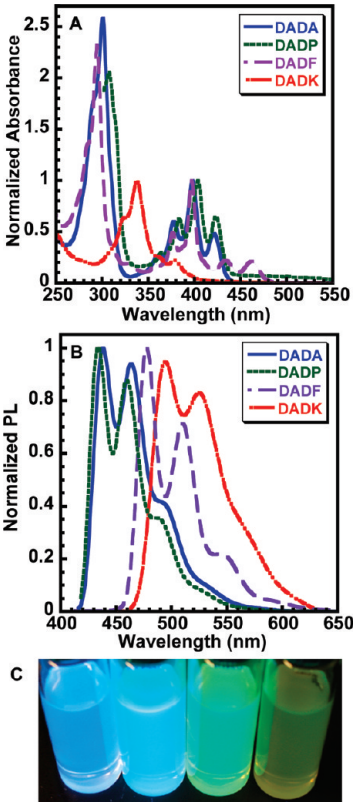

Figure 3. (A) Optical absorption and (B) PL spectra of bisindenoanthrazolines in THF solutions. (C) Photograph of bisindenoanthrazolines in toluene solution under UV irradiation.

corresponds to the 0−2 transition. The absorption maxima (λ_{max}) of DADA, DADP and DADF are 398, 404, 397 nm, respectively; whereas that of DADK (340 nm) is blue-shifted by 58 nm compared to DADA (Table 2).

Figure 3B shows the normalized PL emission spectra of the four BIDAs in dilute THF solution (1×10^{-6} M). The four PL emission spectra have structured bands. DADA and DADP have almost identical blue emission spectra with PL maximum of 438 and 434 nm, respectively, implying that the benzyl groups in DADP have no influence on the transition energies. However, a bathochromic shift of 40 and 56 nm are observed in the PL spectra of DADF and DADK compared to DADA and DADP. The PL emission of DADF and DADK are green and orange with PL maxima of 478 and 494 nm, respectively. When the 0−0 transition in the emission is compared with the 0−0 transition of the corresponding absorption bands, the Stokes shift is small for all the molecules except for DADK. In the case of DADK, there is a large Stokes shift of 114 nm, indicating an intramolecular energy transfer due to carbonyl moieties.[11a,15a] The PL quantum yields of the BIDAs in dilute toluene solution are summarized in Table 2. The PL quantum yields of DADA, DADP, and DADF are 52, 47, and 33%, respectively. However, a significantly lower quantum yield for DADK (3%) was observed, evidence of fluorescence quenching due to the carbonyl moieties.[11a,15a] Figure 3C shows a photograph of the bisindenoanthrazolines in toluene solutions under UV irradiation. Emission spanning blue to yellow is seen in the solutions corresponding to various substituents in bisindenoanthrazoline backbone.

Figure 4A shows the thin film optical absorption spectra of the four BIDAs. The structured absorption bands and the two absorption peaks observed in dilute solution are also seen in evaporated thin films, except for DADK thin film, which has only one broad absorption peak. The thin film absorption bands of DADA, DADP, and DADF are almost identical to those in dilute solution whereas that of DADK has a red shift of 20 nm. The optical band gaps were determined from the onset thin film absorption and are shown in Table 2. The optical band gaps are 2.43 eV for DADF, 2.67 eV for DADA, 2.76 eV for DADP, and 2.99 eV in the case of DADK.

The PL emission spectra of the thin films of BIDAs are shown in Figure 4B. The emission spectra are significantly red-shifted compared to the solution emission spectra by 60−130 nm. In addition, the thin film emission spectra have broad, featureless characteristics. This suggests that the thin film luminescence is from "static" excimer states formed as a result of the π-stacking of the molecules in the solid state.[35] The PL maxima of DADA, DADP, and DADF are summarized in Table 2. DADA and DADP have similar green-yellow emission spectra with PL maxima of 545 and 531 nm, respectively.

(35) (a) Jenekhe, S. A.; Osaheni, J. A. *Science* **1994**, *265*, 765. (b) Osaheni, J. A.; Jenekhe, S. A. *Macromoleclues* **1994**, *27*, 739.

Table 2. Photophysical and Electrochemical Properties of Bisindenoanthrazolines

compd	T_D (°C)	λ_{max}^{abs} (soln) (nm)	λ_{max}^{abs} (film) (nm)	E_g^{opt} (eV)	λ_{max}^{em} (soln) (nm)	λ_{max}^{em} (film) (nm)	ϕ_f (soln)	E_{red}^{onset} (V)	EA (eV)	IP (eV)
DADA	420	398	405	2.67	438	545	0.52	−0.73	3.67	5.73
DADP	418	404	406	2.76	434	531	0.47	−0.75	3.65	5.88
DADF	498	397	403	2.43	478	608	0.33	−0.68	3.72	6.15
DADK	490	340	321	2.99	494	553	0.03	−0.70	3.70	6.69

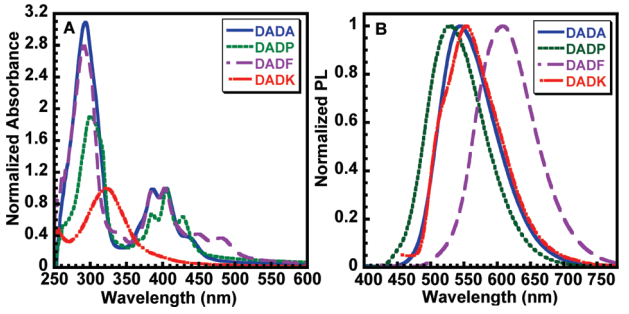

Figure 4. (A) Optical absorption and (B) PL spectra of bisindenoanthrazolines thin films.

Orange emission spectra with PL maximum of 608 nm and green emission spectra with PL maximum of 553 nm were observed for DADF and DADK, respectively.

3.4. Electrochemical Properties. Cyclic voltammetry was performed in millimolar solutions of the BIDAs in 1,2-dichlorobenzene/acetonitrile (10:3 v/v) at 100 °C. The electrochemical data are collected in Table 2. The reduction cyclic voltammograms (CVs) of the four molecules in solution are shown in Figure 5. DADA and DADP show two reduction waves which are quasi-reversible. One reversible reduction wave was observed in the CVs of DADF and DADK. The onset reduction potential of the BIDAs are −0.73, −0.75, −0.68, and −0.70 V (vs SCE) for DADA, DADP, DADF, and DADK, respectively. We note that the reduction potentials of all the four molecules are comparable with a difference of only 0.1 V. It is evident that the heptacyclic bisindenoanthrazolines can be more easily reduced than the tricyclic anthrazolines, which show reversible reduction with onset reduction potential of −1.30 V (vs SCE).[20a] Irreversible oxidation potentials were observed for DADA and DADP with onset oxidation potential of 1.33 and 1.48 V (vs SCE), respectively. However, oxidation potentials were not observed for DADF and DADK. The electron affinity (EA) or LUMO level and ionization potential (IP) or HOMO level were estimated from the onset of either the reduction waves or the oxidation waves in CVs, respectively by using an SCE energy level of −4.4 eV vs vacuum (EA = E_{red}^{onset} + 4.4 eV; IP = E_{ox}^{onset} + 4.4 eV).[20b] The electron affinity was in the range of 3.65−3.72 eV for the series of BIDAs. The ionization potentials (IP) or the HOMO levels for DADA and DADP are 5.73 and 5.88 eV, respectively. We estimated an IP of 6.15 and 6.69 eV for DADF and DADK, respectively, from optical band gap, IP = EA + E_g^{opt}.

The observed electron affinity of ~3.7 eV in the series of BIDA molecules is important and it clearly suggests a good potential for electron transport in these n-type materials. Although the EA and IP values derived from

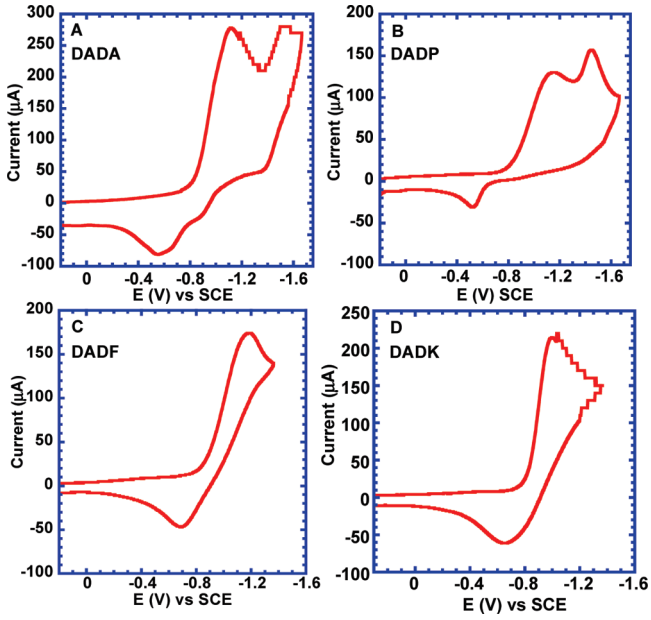

Figure 5. Cyclic voltammograms of (A) DADA; (B) DADP; (C) DADF; and (D) DADK (1.5−3 mM) in 1,2-dichlorobenzene/acetonitrile (10:3 v/v), 0.1 M TBPF6 at 100 °C. Scan rate = 300 mV/s.

cyclic voltammetry can be significantly different from absolute values measured by photoemission techniques,[20b] we believe that our estimates based on an SCE energy level of −4.4 eV relative to vacuum are conservative. We also conclude from the estimated IP values of 5.73−6.69 eV that the bisindenoanthrazolines could not transport holes and indeed would be excellent for blocking holes in OLEDs.

3.5. Self-Assembly of Nanowires. The self-assembly of 1D nanostructures from π-conjugated molecules can be induced by various methods.[30−33] Here, we explored the self-assembly of nanowires (NWs) of the BIDA molecules by the solution-phase route[31,32] and focused on DADF and DADK whose bulk single crystals were previously discussed. DADF nanowires were prepared by adding a solution of 5 mg/mL of DADF in THF into a clean 20 mL vial, followed by 15 mL of methanol. The mixture was allowed to gently stir at room temperature and the nanowires were formed within 15 min. In the case of DADK NWs, they were grown by dissolving 5 mg into hot 12 mL dichlorobenzene and the solution was heated to boiling (181 °C). The solution was slowly cooled to room temperature and left without stirring. DADK NWs were observed after 5 hours.

The solution-phase assembled DADF and DADK NWs were characterized by transmission electron microscopy (TEM), scanning electron microscopy (SEM), and selected area electron diffraction (SAED). The DADF NWs have widths of 100−150 nm and lengths

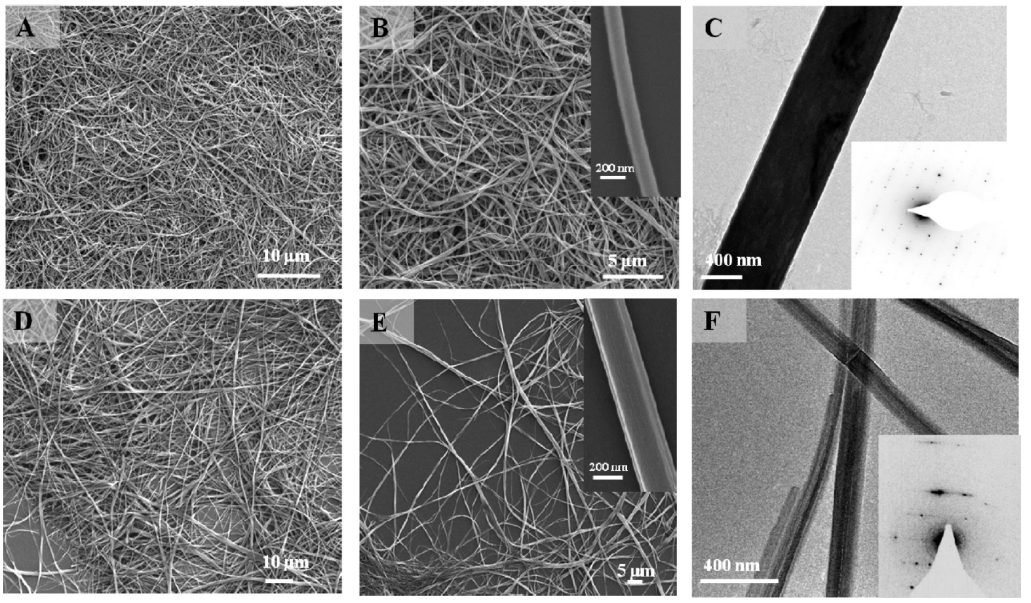

Figure 6. (A, B, D, E) SEM and (C, F) TEM images with corresponding electron diffraction (inset) of (A−C) DADF and (D−F) DADK.

of 10−200 μm, as shown in images A and B in Figure 6. The size of NWs could be varied by adjusting the solution concentration and assembly period. For example, microwires of DADF with width of 1−2 μm were obtained by slow assembly of the molecules in THF during 48 h (see Figure S5C, D in the Supporting Information). Figure 6C shows the TEM image of a single DADF NW and the inset shows an electron diffraction of the single NW. The sharp spots in the SAED pattern clearly demonstrate that the NWs are single-crystalline. DADK NWs have width of 200−250 nm and lengths of several hundred micrometers (Figure 6D, E). The high density of the nanowires as seen in the SEM and TEM images clearly demonstrates that these nanowires can be processed over large areas for potential use in device applications. Figure 6F shows the TEM image of DADK nanowire and the corresponding electron diffraction (inset), which indicates that the nanowires are single-crystalline.

3.6. Electron Transport. The mobility of electrons in films of the bisindenoanthrazolines was evaluated by the space-charge limited current (SCLC) method in ambient conditions. Figure 7 shows the current-density/voltage ($J-V$) characteristics of SCLC devices which have the structure Al/BIDA (< 190 nm)/Al. The electron mobility was extracted by fitting the $J-V$ curves in the near quadratic region according to the modified Mott−Gurney equation[36] (eq. 1)

$$J = \frac{9}{8}\varepsilon\varepsilon_0\mu\frac{V^2}{L^3}\exp\left(0.89\beta\frac{\sqrt{V}}{L}\right) \qquad \text{(eq. 1)}$$

where J is the current density, V is the applied voltage, L is the thickness of active layer, μ is the mobility, ε is the relative permittivity of free space, ε_0 is the permittivity of free space, and β is the field-activation factor (Table 3).[36] The solid lines in Figure 7 represent the best fitting curves in the quadratic SCLC region.

The mobility of electrons was calculated to be 3.84×10^{-4}, 3.07×10^{-5}, 2.29×10^{-6}, 4.33×10^{-7} cm^2/(V s) for DADK, DADA, DADF, and DADP, respectively. The SCLC electron mobility of DADK was the highest observed among the series of molecules. The electron mobility is an order of magnitude higher than that of DADA and 2 orders of magnitude higher than that of DADF. The high mobility of DADK could be explained by the close intermolecular $\pi-\pi$ distance that results in a better intermolecular orbital overlap than DADF. The SCLC electron mobility of DADP was 2 orders of magnitude lower than that of DADA. The charge carrier mobility of DADA and DADK is about one to two orders of magnitude higher than those of conventional electron transport materials such as Alq_3,[37a] oxadiazole derivatives,[37b] and diphenylphenanthroline (BPhen).[37c] The low carrier mobility in DADP could be due to the poor intermolecular interactions as a result of the benzyl groups. Based on the previously discussed EA and IP values for the 4 BIDA molecules the small energy barrier for electron injection from Al (Φ = 4.3 eV)[20b] is small and comparable in all 4 molecules. Thus, the observed 3 orders of magnitude variation in the SCLC electron mobility of the series of BIDAs must be due to variation in the solid-state morphology of the materials. Nevertheless, the fact that a simple substitution in the structure of the bisindenoanthrazolines can translate into a huge variation in charge transport properties is instructive in the design of organic semiconductors.[28c] The observed low carrier mobility

(36) (a) Murgatroyd, P. N. *J. Phys. D* **1970**, *3*, 1488. (b) Mott, N. F.; Gurney, D. *Electronic Processes in Ionic Crystals*; Academic Press: New York, 1970. (c) Campbell, A. J.; Bradley, D. D. C.; Lidzey, D. G. *J. Appl. Phys.* **1997**, *82*, 6326.

(37) (a) Choudhury, K. R.; Yoon, J.-H.; So, F. *Adv. Mater.* **2008**, *20*, 1456. (b) Chu, T.-Y.; Song, O.-K. *Appl. Phys. Lett.* **2007**, *90*, 203512. (c) Khan, M. A.; Xu, W.; Haq, K.-U.; Bai, Y.; Jiang, X. Y.; Zhang, Z. L.; Zhu, W. Q.; Zhang, Z. L.; Zhu, W. Q. *J. Appl. Phys.* **2008**, *103*, 014509.

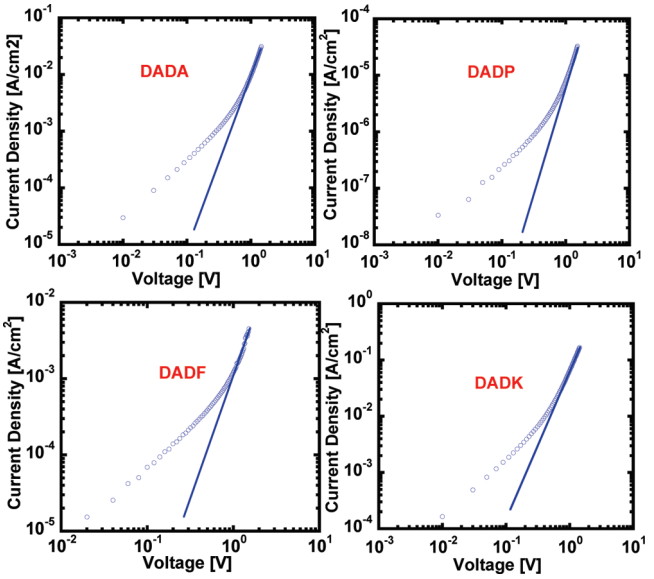

Figure 7. Current density, J vs V of Al/bisindenoanthrazoline/Al devices in ambient conditions. The solid lines represent SCLC model with field-dependent mobility.

Table 3. SCLC Characteristics of Bisindenoanthrazolines

compd	L (nm)	β (cm/V)$^{1/2}$	E_{max} (V/cm)	μ_e (E = 0) (cm^2/V s)
DADA	182	8.9×10^{-3}	8.0×10^{4}	3.1×10^{-5}
DADP	179	1.1×10^{-2}	8.6×10^{4}	4.3×10^{-7}
DADF	144	7.9×10^{-3}	1.1×10^{5}	2.3×10^{-6}
DADK	161	4.9×10^{-3}	8.4×10^{4}	3.8×10^{-4}

measured by SCLC could be due to the fact that the mobility is not measured along the π-stacking direction, which is the optimum direction for charge transport. This is because the direction of charge transport measured by SCLC method is perpendicular to the substrate, whereas the π-stacking direction is generally parallel to the substrate.

Initial attempts to measure the electron mobility of single-crystalline self-assembled nanowires of DADK using the field effect transistor geometry[32a,e] were unsuccessful. This lack of n-channel field effect charge transport may be due to the high injection barrier between the gold source/drain electrodes (Φ = −5.1 eV) and the LUMO level of DADK (−3.7 eV). In addition, n-channel transport is highly unstable in ambient conditions, especially in bottom contact and bottom gate devices used in our study.

3.7. Electroluminescence. The BIDAs were explored in electroluminescent (EL) devices both as emissive materials in OLEDs and as electron transport materials in phosphorescent OLEDs (PhOLEDs). The following three different device structures incorporating a BIDA as the emitter were fabricated and tested: ITO/PEDOT:PSS/BIDA/LiF/Al (diode I); ITO/PEDOT:PSS/TAPC/BIDA/LiF/Al (diode II); and ITO/PEDOT:PSS/TAPC/BIDA/TPBI/LiF/Al (diode III). The EL properties of diodes I−III are summarized in Tables 4 and 5. The EL spectra of diode III incorporating DADA, DADP, or DADF as the emissive layer and diode II using DADK as the emitter are shown in Figure 8A. The EL spectra of DADA, DADP, and DADF are very similar to their respective PL spectra with EL maximum of 547, 540, and 608 nm, respectively. The EL spectra of these three BIDA molecules (DADA, DADP, DADF) are very similar with the PL spectra, which as discussed above, originated from excimer emission.[35] In contrast, the EL spectrum of DADK has a peak at 685 nm, which is significantly different from the PL emission maximum at 553 nm. We propose that EL emission from DADK-based diode II results from the recombination of charges at the interface of the hole transport layer (TAPC) and DADK layer and thus exciplex formation.[38] We attempted to directly confirm this hypothesis by obtaining the PL emission spectrum of a TAPC/DADK bilayer. However, the PL emission spectrum from the bilayer was different from the EL spectrum. The CIE coordinates of the EL emission of the four compounds are shown in Figure 8B. Greenish-yellow EL with CIE coordinates of [(0.33, 0.57), (0.32, 0.56)] was observed for DADA and DADP, whereas orange with CIE coordinates (0.53, 0.46) and red EL with CIE coordinates of (0.65, 0.35) were observed in DADF and DADK, respectively.

Figure 9A−D shows the current density−voltage and luminance−voltage characteristics of diode III based on DADA, DADP, DADF, or DADK as the emissive layer. The turn-on voltage of the three diodes was in the range of 3.8−4.0 V, indicating low charge injection barriers. Device III gave the best performance for DADA, DADP and DADF as expected from the incorporation of both a TAPC hole transport layer (HTL) and a TPBI hole blocking layer (HBL). Among the bisindenoanthrazolines, DADA gave the best performance as an emissive material in EL diodes, giving a maximum brightness of 7610 cd/m^2, an EQE of 0.66%, and a luminous efficiency of 2.1 cd/A (Table 5). The maximum luminous efficiency of diode III containing DADA was 6.6 cd/A with an EQE of 2.0% at a brightness of 936 cd/m^2 (Table 4). In the case of DADP, the maximum brightness was 5040 cd/m^2 with an EQE of 0.55% and a luminous efficiency of 1.7 cd/A (Table 5). The maximum efficiency of diode III containing DADP was 4.8 cd/A at a brightness of 604 cd/m^2 with an EQE of 1.55% (Table 4). The maximum brightness of diode III containing DADF was 5110 cd/m^2 with an EQE of 0.42% and a current efficiency of 1.5 cd/A. EL performance of diodes I−II containing DADK was very poor. EL from diode III containing DADK did not originate from DADK but rather from an exciplex emission.[35,38] An alternative possibility is that the red EL of DADK originates from electrophosphorescence. However, additional photophysical studies at low temperatures will be required to confirm such an unprecedent phenomenon in a molecule without a heavy atom. The higher brightness and efficiency of DADA compared to DADP could be explained by its relatively higher fluorescence quantum yield and higher electron mobility. Single-layer diode I further confirms that DADA is a

(38) (a) Jenekhe, S. A. *Adv. Mater.* **1995**, *7*, 309. (b) Kulkarni, A. P.; Jenekhe, S. A. *J. Phys. Chem. C* **2008**, *112*, 5174.

Table 4. EL Properties of Bisindenoanthrazolines[a]

compd	diode	V_{on}[b]	drive voltage (V)	current density (mA/cm^2)	luminance (cd/m^2)	luminous efficiency (cd/A) [EQE[c] %]	λ_{max}^{EL} (nm)
DADP	I	5.0	6.0	452	2	0.05 [0.0002]	539
	II	2.8	7.0	217	1850	0.85 [0.32]	540
			5.2	*15*	*335*	*2.2 [0.71]*	
	III	4.5	11.1	100	2410	2.4 [0.79]	540
			9.1	*13*	*604*	*4.8 [1.55]*	
DADA	I	4.0	8.7	410	584	0.14 [0.045]	545
	II	3.0	10.8	215	2140	1.00 [0.30]	547
			8.5	*31*	*604*	*2.0 [0.60]*	
	III	3.8	9.3	91	3840	4.2 [1.29]	547
			7.7	*14*	*936*	*6.6 [2.03]*	
DADF	I	3.8	7.5	388	189	0.05 [0.022]	599
	II	2.8	8.5	361	912	0.25 [0.11]	601
			5.6	*36*	*102*	*0.29 [0.13]*	
	III	4.0	10.6	266	3400	1.3 [0.58]	601
			9.0	*75*	*1330*	*1.8 [0.81]*	
DADK	I	4.0	5.6	266	1	0.0005 [-]	683
	II	3.0	7.9	449	37	0.008 [-]	685
			5.4	*66*	*9*	*0.01* [-]	
	III[d]						

[a] Values in italics correspond to those for maximum device efficiencies at a practical brightness of at least 100 cd/m^2 except values in DADK case. [b] Turn-on voltage (at which EL is visible to the eye). [c] EQE = External quantum efficiency.[20d,e] [d] EL from diode III did not originate from DADK. The structure of device III is ITO/PEDOT(50 nm)/TAPC (20 nm)/BIDA (20 nm)/TPBI (20 nm)/LiF (2 nm)/Al.

Table 5. Device III Characteristics with Maximum Brightness [a]

compd	V_{on} (V)	drive voltage (V)	current density (mA/cm^2)	luminance (cd/m^2)	luminous efficiency (cd/A) [EQE %]	λ_{max}^{EL} (nm)
DADP	4.0	9.8	290	5040	1.7 [0.55]	540
DADA	3.8	9.1	367	7610	2.1 [0.66]	547
DADF	4.0	10.4	349	5110	1.5 [0.42]	601

[a] Device structure is ITO/PEDOT(50 nm)/TAPC (10 nm)/BIDA(20 nm)/TPBI (20 nm)/LiF (2 nm)/Al.

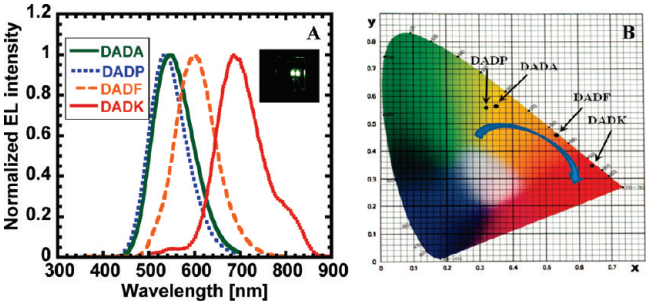

Figure 8. (A) Normalized EL spectra of bisindenoanthrazolines (inset is a photo of a DADA-based device III). (B) CIE coordinates of the EL spectra of device III.

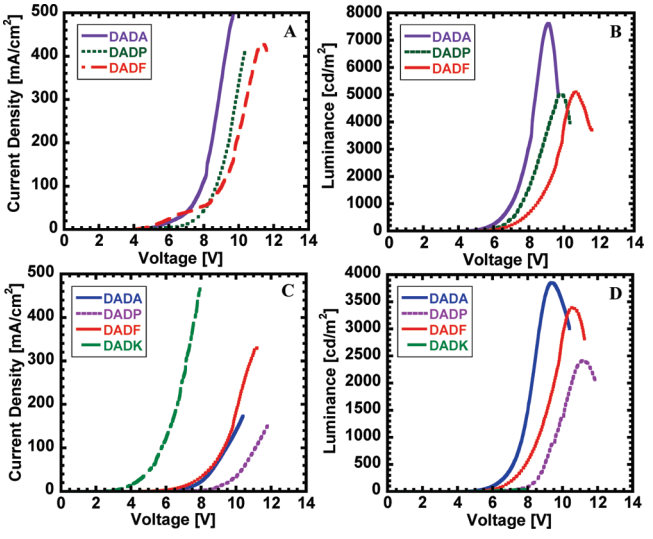

Figure 9. (A) Current density−voltage and (B) luminance−voltage characteristics of diode III with device geometry of: ITO/PEDOT(50 nm)/TAPC (20 nm)/BIDA (20 nm)/TPBI (20 nm)/LiF (2 nm)/Al. (C) Current density−voltage and (D) luminance−voltage characteristics of diode III with device geometry of: ITO/PEDOT(50 nm)/TAPC (10 nm)/BIDA (20 nm)/TPBI (20 nm)/LiF (2 nm)/Al.

superior electron transport material than DADP; a brightness of 584 cd/m^2 was obtained from DADA compared to a brightness of 2 cd/m^2 from DADP. The low luminous efficiency and brightness in diodes I−III containing DADF and DADK can be explained by the low fluorescence quantum yield in the materials.

3.8. Electron Transport Properties of BIDAs in PhOLEDs. We also evaluated the new bisindenoanthrazolines as electron transport materials (ETMs) in phosphorescent OLEDs (PhOLEDs). A blend of poly(*N*-vinylcarbazole) (PVK) and 1,3-bis(2-(4-*tert*-butylphenyl)-1,3,4-oxadiazo-5-yl)benzene (OXD-7) (PVK:OXD-7 = 60:40 wt/wt) served as the host to which a 1.0 wt % *fac*-tris(2-phenylpyridine)iridium (Ir(ppy)$_3$) green triplet emitter was doped, resulting in an emissive polymer layer (EML). Five sets of devices were investigated, including: ITO/PEDOT:PSS/EML/LiF/Al without an electron-transport layer (ETL) which served as a reference. Four diodes, each containing a BIDA molecule as an ETL, were fabricated with the structure: ITO/PEDOT:PSS/EML/ETL/LiF/Al. The normalized EL emission spectra of the PhOLEDs are shown in Figure 10A. At all drive voltages, EL emission was observed only from the green triplet emitter, which has

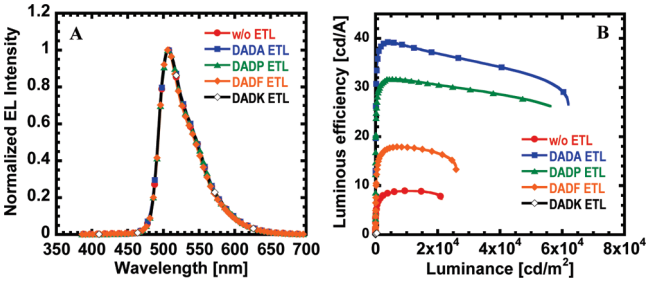

Figure 10. (A) Normalized EL spectra of the PhOLEDs at a drive voltage of 17.6−20.4 V. (B) Luminous efficiency−luminance (*LE*−*L*) curves of PhOLEDs with the structures: ITO/PEDOT:PSS/EML/LiF/Al and ITO/PEDOT:PSS/EML/BIDA (ETL)/LiF/Al.

Table 6. PhOLEDs Performances Using Bisindenoanthrazolines as ETMs[a]

ETL	V_{on} (V)	drive voltage (V)	current density (mA/cm^2)	luminance (cd/m^2)	luminous efficiency (cd/A) [EQE %]
	10.8	18.9	290	21 300	7.3 [2.3]
		17.9	*116*	*10 326*	*8.9* [*2.9*]
DADA	8.1	16.9	233	62 000	26.6 [8.7]
		13.5	*11.8*	*4270*	*39.2* [*12.6*]
DADP	8.2	16.8	215	56 300	26.2 [8.5]
		13.6	*14.1*	*4470*	*31.7* [*10.2*]
DADF	9.5	17.6	194	25 900	13.3 [4.3]
		15.6	*38.5*	*6900*	*17.9* [*5.8*]
DADK	12.0	20.4	233	630	0.27 [0.13]
		19.5	*136*	*460*	*0.34* [*0.16*]

[a] Values in italics correspond to those for maximum device efficiencies.

a maximum emission peak at 512 nm due to the $Ir(ppy)_3$. EL emission from the BIDA ETMs was not observed. This clearly means that the BIDA molecules function exclusively as electron-transport materials, efficiently confining charge carriers and excitons within the EML.[39]

The luminous efficiency-luminance (*LE*−*V*) curves of the PhOLEDs are shown in Figure 10B and the associated device performance are collected in Table 6. PhOLEDs using a DADA ETL showed the highest brightness of 62 000 cd/m^2 and the highest luminous efficiency (*LE*) value of 39.2 cd/A (EQE of 12.6%) at a brightness of 4270 cd/m^2, which is almost 4-fold higher than PhOLEDs without an ETL. DADP ETL also enhanced the PhOLED performance, showing a LE value of 31.7 cd/A (EQE of 10.2%) at a brightness of 4470 cd/m^2. PhOLEDs with a DADF as ETL also showed improved performance (Table 6). Unexpectedly, PhOLEDs using DADK as an ETL showed a severely quenched EL with a brightness of only 630 cd/m^2, which is 2 orders of magnitude less than the device without an ETL. This means that whereas DADA, DADP, and DADF are good ETMs for use in PhOLEDs, DADK is not an effective ETL material. We note that it is better for an electron-transport layer to have an amorphous morphology.[20b] Aggregation of the molecules of an ETM and crystallization of the ETL can result in poor charge-injection at the interface. The strong intermolecular interactions in DADF and DADK were already evident in their self-assembled nanostructures discussed above. This could explain the poor performance of PhOLEDs based on DADK and DADF ETLs. Overall, these results demonstrate that DADA and DADP are very promising electron-transport materials for applications in PhOLEDs, whereas DADF and DADK are not as promising apparently because of their tendency to crystallize readily.

(39) Earmme, T.; Ahmed, E.; Jenekhe, S. A. *J. Phys. Chem. C* **2009**, *113*, 18448.

4. Conclusions

A novel π-conjugated heptacylic framework has been synthesized and found to be a new class of n-type organic semiconductors. Single-crystal X-ray diffraction showed that the novel heptacyclic framework is planar and leads to a slipped face-to-face π-stacking. The high electron affinity (3.7 eV) and high electron mobility (1×10^{-7} to 1×10^{-4} cm^2/(V s)) of the bisindenoanthrazolines makes them attractive candidates for electron transport in organic electronics. Two members of this class of ladder oligomers (DADF and DADK) were shown to assemble in solution into single-crystal nanowires with widths of 100−250 nm and lengths of 10−200 μm. The bisindenoanthrazoline emitted electroluminescence with a high brightness (7610 cd/m^2), and high efficiency (6.6 cd/A with EQE of 2.0% at a brightness of 936 cd/m^2). Some of the BIDAs (DADA and DADP) were excellent electron-transport materials in realizing high performance phosphorescent OLEDs, a brightness of 62 000 cd/m^2 and luminous efficiency of 39.2 cd/A at a brightness of 4270 cd/m^2 was achieved in green PhOLEDs. These results demonstrate that the bisindenoanthrazolines is a promising new class of n-type semiconductors for organic electronics and optoelectronics.

Acknowledgment. The synthesis and properties of n-type organic semiconductors were supported by the NSF (DMR-0805259 and DMR-0120967) and the assembly and characterization of nanowires was supported by the ONR (N00014-08-1-1148). E.A. received a UNCF/Merck Graduate Science Research Dissertation Fellowship. G.R. received a UIF Fellowship from the Center for Nanotechnology. Part of this work was conducted at the University of Washington NanoTech User Facility, a member of the NSF National Nanotechnology Infrastructure Network (NNIN). We also thank John Freudenthal for determining the crystal structures.

Supporting Information Available: Single-crystal X-ray diffraction files (CIF); ^{1}H NMR and SEM and TEM images (PDF). This material is available free of charge via the Internet at http://pubs.acs.org.